Experimental Investigation of the Aerodynamic Interaction Between Overlapping Propellers in Tandem for eVTOL Airplane-Mode Flight Conditions

Alex Zanotti*, Davide Algarotti, Donato Grassi, Luca Riccobene,
Politecnico di Milano, Dipartimento di Scienze e Tecnologie Aerospaziali,
via La Masa 34, 20156, Milano - Italy
* alex.zanotti@polimi.it

Abstract

The latest trends of Urban Air Mobility (UAM) pushed the aeronautical community towards the eVTOL concept, i.e. electrical vertical take-off and landing aircraft. Electrical power, tilt-wing configuration and multiple propellers in tandem configuration (i.e. with the propellers placed one after the other) are the key features of such concept. In particular, the presence of multiple propellers working at close range introduces a new challenge, i.e. the investigation of the aerodynamic interaction between front propeller slipstreams and rear propellers. The present work aims to investigate the main physical aspects of this phenomenon in a typical eVTOL configuration in airplane mode. A dedicated wind tunnel testing campaign was performed to investigate deeply the interaction between two co-rotating tandem propellers at fixed axial distance and variable lateral separation. The tests included both thrust and torque measurements of the propellers and Particle Image Velocimetry (PIV) surveys. Load measurements showed a significant loss in the rear propeller performance as a function of the overlapping ratio between the propellers. Furthermore a dedicated spectral analysis of wind tunnel thrust signals outlined high amplitude fluctuations in partial overlapping configurations. The collected experimental results represent a reference database for the validation of numerical codes implemented during the design phase of such vehicles. In particular, some experimental data were compared with results obtained by the mid-fidelity aerodynamic solver DUST relying upon Vortex Particle Method (VPM) in order to enhance the comprehension of the phenomenon. The analysis of the numerical results allowed to access the flow behaviour involving the front propeller slipstream and the rear propeller disk, which is responsible of the massive losses experienced by the rear propeller.

Notation

C_P	power coefficient, $= P/(\rho n^3 D^5)$
C_T	thrust coefficient $= T/(\rho n^2 D^4)$
D	propeller diameter
J	advance ratio $= V_\infty/(nD)$
L_x	axial distance between propeller disks
L_y	lateral distance between propeller axis
M_t	tip Mach number
n	rotational speed [rad/s]
P	propeller power [W]
R	propeller blade radius [m]
Re_D	Reynolds number based on propeller diameter
T	propeller thrust [N]
u	freestream velocity component [m/s]
v	vertical velocity component [m/s]
w	out-of-plane velocity component [m/s]
V_∞	free-stream velocity
ρ	air density [kg/m^3]
ψ	blade azimuthal angle [deg]
ω_z	out-of-plane vorticity component [1/s]

1 INTRODUCTION

The great challenge to create a sustainable world involves also air transport. Indeed, in the next future the growth of metropolitan areas will provide a wide increase of urban traffic, thus having a great impact on pollution and gas emission. In addition to the great effort spent by automotive companies for an effective electrification of ground transport vehicles, the aeronautical world is also looking to the development of unconventional VTOL aircraft based on electric distributed propulsion, called eVTOLs, to be considered, in the next future, as a sustainable alternative to ground transportation in overcrowded metropolitan areas [1]. This futuristic vision opened the market of urban air mobility (UAM). Thus, in recent years, a large number of startup companies as well as aerospace industries devoted their effort to the design of novel short-range VTOL aircraft aimed to transportation in urban areas. Despite the architectures of these novel air vehicles are rather diverse, as shown in [2, 3], the common feature that can be clearly distinguished is related to the use of multiple propellers, typically mounted on a

Presented at the 48th European Rotorcraft Forum, Winterthur, Switzerland, 6-8 September, 2022

single or dual lifting surface. Consequently, a critical aspect to be thoroughly investigated is to evaluate possible detrimental effects on performance, handling qualities and noise impact of these brand new aircraft concepts due to aerodynamic interaction between propellers. Considering the typical layout of eVTOL aircraft [2, 3], two main kind of propeller-propeller aerodynamic interaction could occur, i.e. with adjacent propellers in side-by-side configuration (propeller disks lying on same plane) or with propellers disks lying on planes at a certain axial distance with a degree of overlapping between them. The latter type of aerodynamic interaction occurs, particularly, in airplane-mode flight condition for eVTOLs architectures characterised by two rows of propellers positioned on tandem lifting surfaces (see for instance the Airbus Vahana aircraft [4] shown in Fig. 1). Indeed, in cruise flight condition, the fore propeller slipstream invests the rear propeller blades, thus affecting propellers performance. Consequently, the investigation of the effects of aerodynamic interaction between two overlapping propellers in tandem configuration represents an essential aspect to drive the aerodynamic design of such eVTOLs.

Figure 1: Overlapping propellers in tandem on Airbus Vahana layout (courtesy of A^3 by Airbus LLC).

Despite literature review highlights a comprehensive effort dedicated to the investigation of rotor-rotor aerodynamic interaction, these studies are mainly aimed to helicopter applications [5, 6] or to side-by-side propellers [7, 8] in hover flight conditions. Consequently, there is a certain lack in literature of experimental activities aimed to gain knowledge about aerodynamic interactions between overlapping tandem propellers configurations typical of eVTOL aircraft in forward flight conditions. The present paper describes an experimental activity performed at Politecnico di Milano aimed to reproduce the tandem propellers configurations investigated in the preliminary numerical work performed by Zanotti et al. [9] using the mid-fidelity numerical solver DUST [10] and presented at 47^{th} European Rotorcraft Forum. The experimental activity was aimed to provide a robust validation of the mid-fidelity numerical approach implemented in DUST and to be used for a thorough investigation of this interactional aerodynamics problem. Some comparisons of the experimental results with numerical simulations performed with DUST purposely tuned to fit the wind tunnel tests parameters are presented in this paper. Moreover, the present experimental database was also aimed to fill the gap in literature related to experimental studies investigating interacting flow mechanisms occurring in airplane-mode flight condition of eVTOL aircraft.

2 EXPERIMENTAL SETUP

A systematic series of wind tunnel tests were performed at the *S. De Ponte* wind tunnel of Politecnico di Milano (1 m $\times$ 1.5 m test section) over two propeller models in tandem configuration by changing their lateral separation distance (L_y) at fixed axial distance (L_x). Two propeller models were purposely designed and manufactured for the wind tunnel test campaign (see the model layout in Fig. 2a).

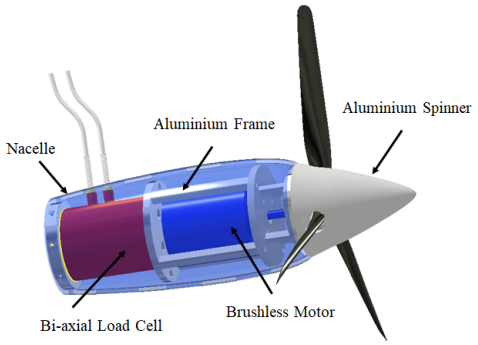

(a)

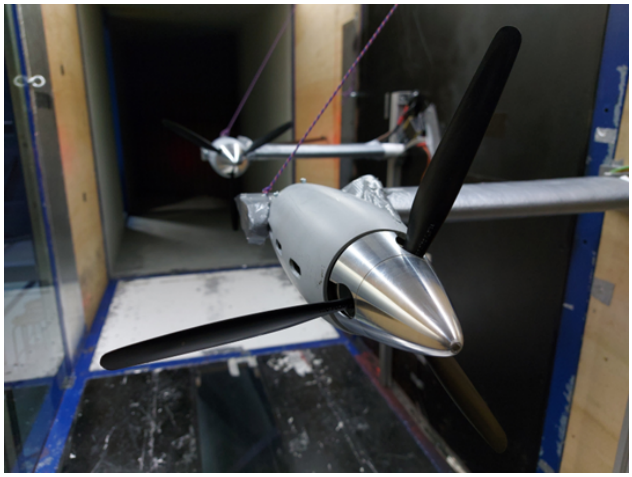

(b)

Figure 2: (a) Propeller model layout, (b) Set up of tandem propellers at the *S. De Ponte* wind tunnel.

The propeller hub was designed using hobby-grade components. In particular, a three-bladed hub equipped with 150 mm radius blades was used. An internal aluminium frame was designed to support the propeller driving system and a bi-axial strain gauge load cell. The propeller was driven by a brushless motor (5.3 kW continuous power) with shaft connected directly to propeller hub.

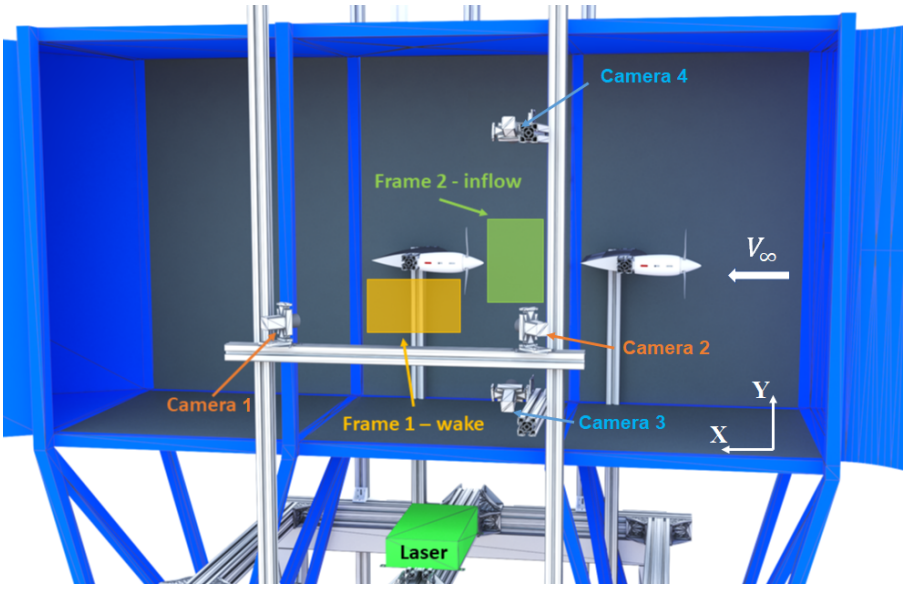

Figure 3: PIV set up for stereoscopic measurements on tandem propellers interaction at *S. De Ponte* wind tunnel.

A polycarbonate nacelle was manufactured using FDM technique and mounted on the internal metallic frame to shield both the motor and the load cell. The propeller models were set up in the wind tunnel test section using metallic frames made by 30 mm $\times$ 30 mm squared section aluminium struts (see Fig. 2b). A NACA 0025 airfoil shaped faring made by polystyrene was installed on the aluminium struts supporting the propellers. The two propellers were mounted in tandem configuration with an axial distance (L_x) between the propellers disk equal to 5 rotor radii to reproduce a typical Vahana-like layout. The aluminium strut attached to one of the lateral walls of the wind tunnel test section, acting as a rail, enabled to modify the lateral separation distance between the models.

Wind tunnel tests included loads measurements (thrust and torque) to evaluate, particularly, the effects on rear propeller performance provided by aerodynamic interaction of front propeller slipstream. A FUTEK MBA500 strain gauge bi-axial load cell (50 lbs F.S.) mounted inside each nacelle was used to measure thrust and torque of each propeller. The load cell has a F.S. range of ±50 lbs for thrust and of ±50 lbs-in for torque, with ±0.25% R.O. non-linearity and ±0.05% R.O. non-repeatability.

The flow field around twin propellers configurations were investigated through stereo Particle Image Velocimetry (sPIV) technique. Two pairs of double-shutter cameras in stereoscopic mode were used to frame two different flow regions, respectively at inflow and in the near wake of the rear propeller (see PIV instrumentation set up in Fig. 3). The first camera pairs consisted of ILA.PIV.sCMOS CLHS cameras by Canon (Camera 1 and Camera 2 in Fig. 3) having a resolution of 2560 x 2160 pixels, 16 bit dynamic range and were used to analyse the wake of the rear propeller in detail. The second camera pairs consisted of Imperx ICL-B1921M CCD cameras (Camera 3 and Camera 4 in Fig. 3) with 12-bit 1952 × 1112 pixel array and were used to investigate the inflow of the rear propeller. The area of investigation for the inflow was 70 mm wide and 336 mm high, while the windows for the wake was 190 mm wide and 282 mm high. PIV surveys were performed both in free-run condition of the propellers and phase-locked with the azimuthal blade angle of the rear propeller.

The advance ratio range selected for the tests was aimed to evaluate interactional effects from a moderate to a fast cruise flight speed of eVTOLs aircraft flying in urban environment [2, 3], while the propellers rotated at fixed 7050 RPM to reproduce a typical tip Mach number, i.e. $M_t = 0.325$, of full-scale eVTOL aircraft propellers in cruise flight condition [1, 11, 4]. The blade pitch angle evaluated at 75%R of both propellers models was fixed to 26.5° for all the tests. Preliminary tests were performed over a single propeller (i.e. rear model) to characterise a reference aerodynamic performance for the evaluation of interactional effects by comparison with tandem propellers tests results. Stereo PIV surveys were performed for some selected test conditions, particularly focused on a typical target cruise flight velocity of an eVTOL aircraft in urban environment, i.e about 100 km per hour corresponding to advance ratio J equal to 0.8. More details on the experimental set up can be found in [12].

3 RESULTS AND DISCUSSION

This section discusses the main results obtained from the experimental campaign in terms of aerodynamic performance coefficients and flow field analysis. Figure 4 shows the averaged thrust coefficient and power coefficient of the rear propeller as a function of the advance ratio for each tested lateral separation distance L_y. The same plot reports the experimental curves evaluated for the single propeller as a reference to evaluate the impact of the aerody-

namic interaction on tandem propeller performance. Each test point was measured four times and 95% simultaneous confidence bands were calculated based on these four repetitions and plotted as errorbars on the performance curves comparison. As clearly visible from the curves comparison, a strong decrease of the rear propeller performance occurs while reducing the lateral separation distance between the propellers. This behaviour is similar for both thrust and power coefficients in the whole range of advance ratio.

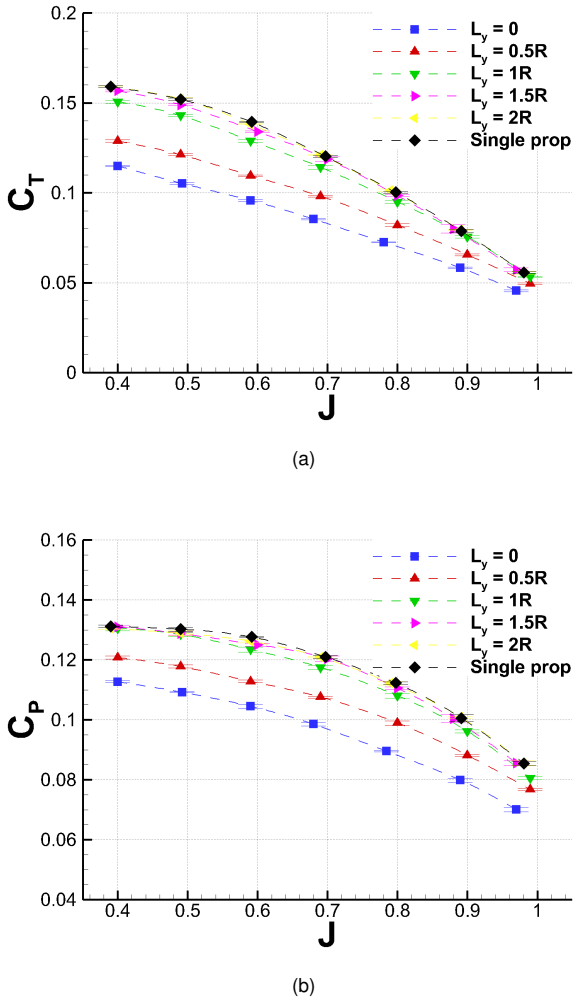

Figure 4: Comparison of the rear propeller experimental performance for tandem propellers configurations, L_x = 5R, $Re_D = 1.96 \cdot 10^6$, $M_t = 0.325$.

The most detrimental condition is the coaxial configuration (i.e. L_y = 0) where the propellers are completely overlapped and the front propeller slipstream is fully impinging on the rear propeller disk. As far as the degree of overlap between the propellers is reduced, the effects on the rear propeller performance decrease and becomes gradually negligible when the degree of overlap becomes zero, i.e. L_y = 2R. Indeed, the performance of the rear propeller approaches the isolated propeller one, since the lateral separation is such that the wake produced by the front propeller not influences the rear propeller inflow. Moreover, the decrease of performance is not proportional to the lateral separation distance reduction between the two propellers. Indeed, a larger reduction of performance is found in the range between $0 < L_y < 1R$ compared to the range between $1R < L_y < 2R$, where the losses on rear propeller performance are smaller. These outcomes related to the analysis of the rear propeller performance are in quite accordance with the experimental results obtained by Stokkermans et. al [13].

An extensive analysis of the interaction effects on the rear propeller is provided for advance ratio J = 0.8, reproducing a typical target cruise flight velocity of an eVTOL aircraft in urban environment, i.e about 100 km per hour.

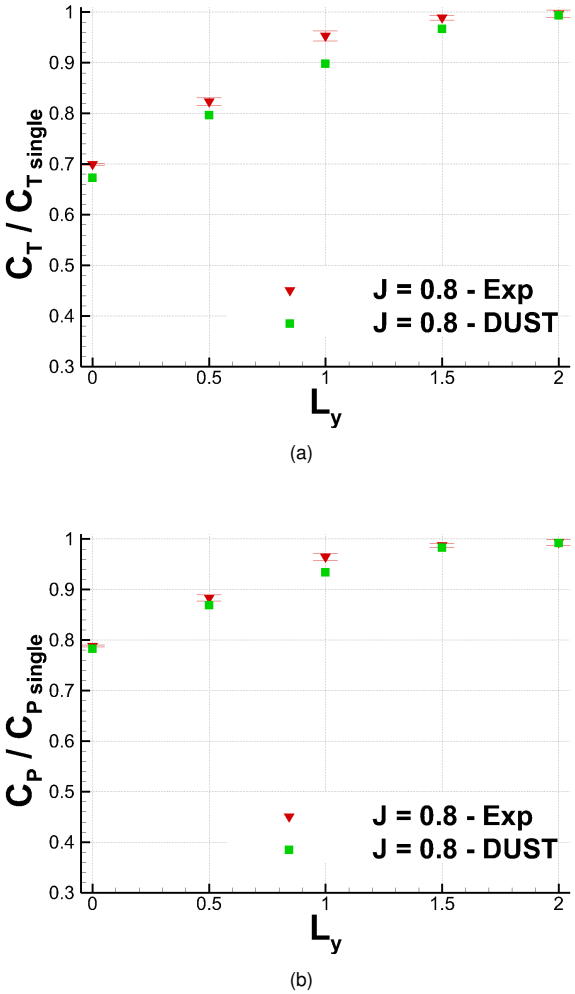

Figure 5: Comparison of the rear propeller performance evaluated with experiments and numerical simulations for tandem propellers configurations at J = 0.8, L_x = 5R, $Re_D = 1.96 \cdot 10^6$, $M_t = 0.325$.

This condition was also considered by the numerical simulations performed with DUST that will be compared in the following to experimental data to assess the robustness of the mid-fidelity numerical approach used to represent

such a complex interactional problem and to enhance the physical comprehension of the performance results. The details of the numerical model used to simulate the tandem propeller configuration are described in [14, 15, 16, 12]. In particular, the propellers blades were modeled in DUST with lifting lines elements, while the spinner-nacelle surface with surface panels [10].

Figure 5 shows the comparison of the numerical and experimental thrust and power coefficients plotted against the lateral separation distance L_y for advance ratio J = 0.8. The performance coefficients were normalised with respect to the single propeller values. Numerical results show good agreement with experimental results over the whole range of tested configurations. As a matter of fact, the maximum gap between experimental and numerical normalised performance coefficients was found to be less than 5% and 3% respectively for thrust and power coefficients. Thus, the mid-fidelity numerical tool DUST can be considered appropriate to describe the aerodynamic interactional effects connected with this problem. Later on, numerical results will be, indeed, used to provide additional insights to the flow physics in order to enhance the comprehension of the aerodynamic interaction between the two propellers with different degree of disks overlapping.

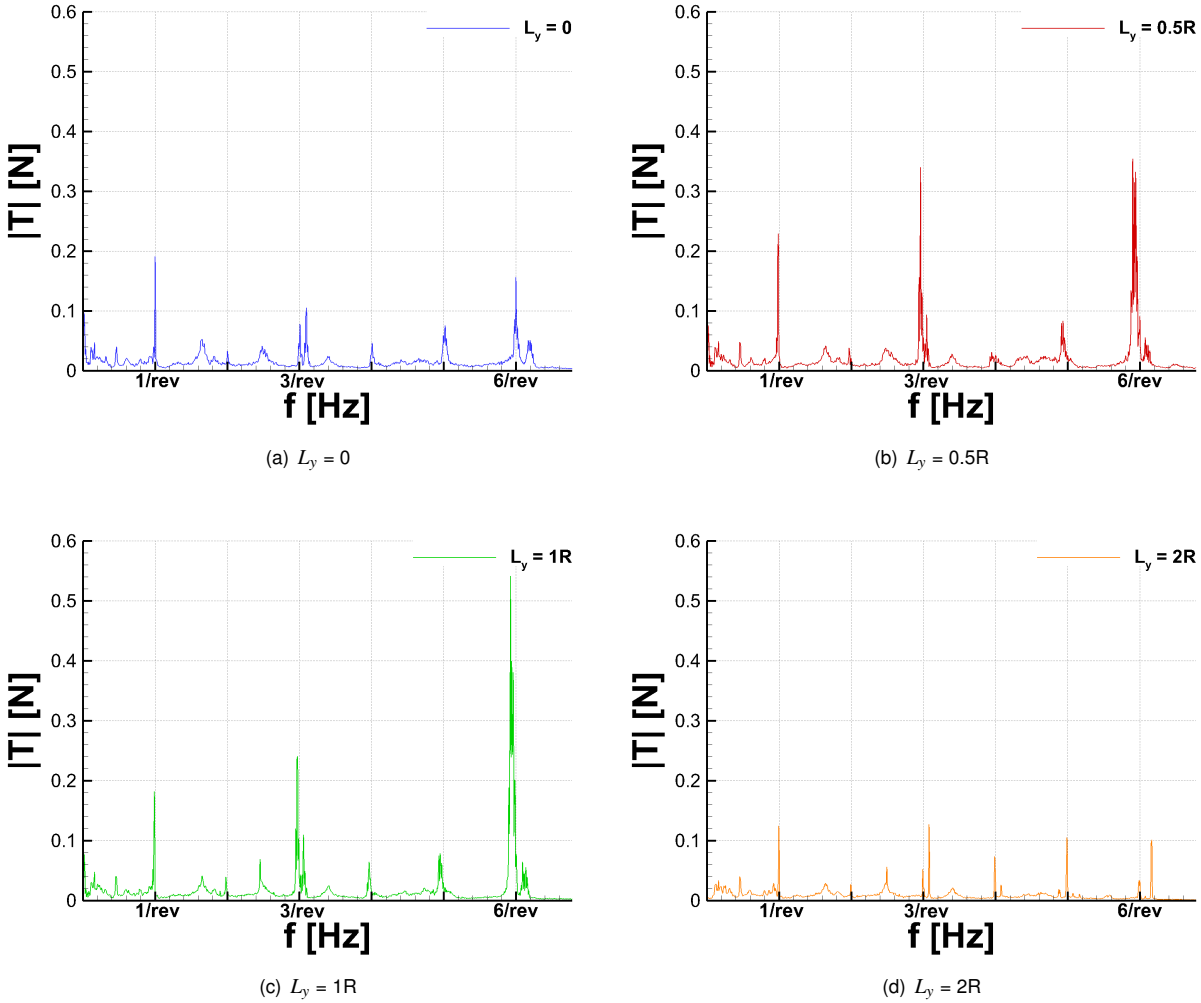

(a) L_y = 0 (b) L_y = 0.5R

(c) L_y = 1R (d) L_y = 2R

Figure 6: Comparison of the measured rear propeller thrust spectra at J = 0.8, L_x = 5R, $Re_D = 1.96 \cdot 10^6$, $M_t = 0.325$.

Both the normalised thrust and power coefficients computed at L_y = 2R resume unity for J = 0.8 confirming that the aerodynamic interaction effects for such configuration are negligible. Increasing the degree of overlap between the propellers up to the configuration with L_y = 1R the performance losses are limited to few percents. Increasing the overlap further, a rapid divergence of the curves is found. In the co-axial configuration experimental results provide a loss on rear propeller performance of nearly 30% of the thrust coefficient and 20% of the power coefficient. Moreover, the experimental data shows an higher level of errorbars for both the rear propeller thrust and power coefficients occurring at L_y = 1R. This configuration, characterised by the overlapping of almost half propeller disk is

characterised by the highest loads fluctuations on the rear propeller blades, while reducing or increasing the degree of overlap between the propellers disks the loads fluctuations decrease. This feature is confirmed by the representation of the rear propeller sectional lift coefficient along the rotor revolution computed by numerical simulations with DUST presented in the past works [14, 15].

The analysis of the spectra of rear propeller thrust signals measured at advance ratio J = 0.8 for different lateral distances of the propellers confirms again that the interaction effects become stronger as the degree of overlap between the two propellers decreases. As during wind tunnel test sessions the two three-bladed propellers were not synchronised in term of blade azimuthal position, the interactional effects can be considered related to the 6/rev peaks in the thrust signal spectra comparison shown in Fig. 6. In particular, the amplitude of the 6/rev peaks of measured thrust increases between L_y = 0 to L_y = 1R, proving that this latter configuration presents the highest level of blade loads fluctuations. This latter result highlighted that possible severe issues in terms of acoustic impact that could occur for vehicle configurations considering partial overlapping tandem propellers disks.

A complete overview of the flow physics involved in the aerodynamic interaction between tandem propellers is provided by the analysis of the flow fields evaluated through PIV surveys and DUST numerical simulations results. In particular, the results presented in the following figures were obtained at J = 0.8 for some specific tandem propellers configurations, i.e. L_y = 0, L_y = 0.5R, L_y = 1R. In particular, PIV results were here ensemble-averaged over the free-run surveys data, while numerical flow fields were here averaged over the time steps of the last computed rotor revolution.

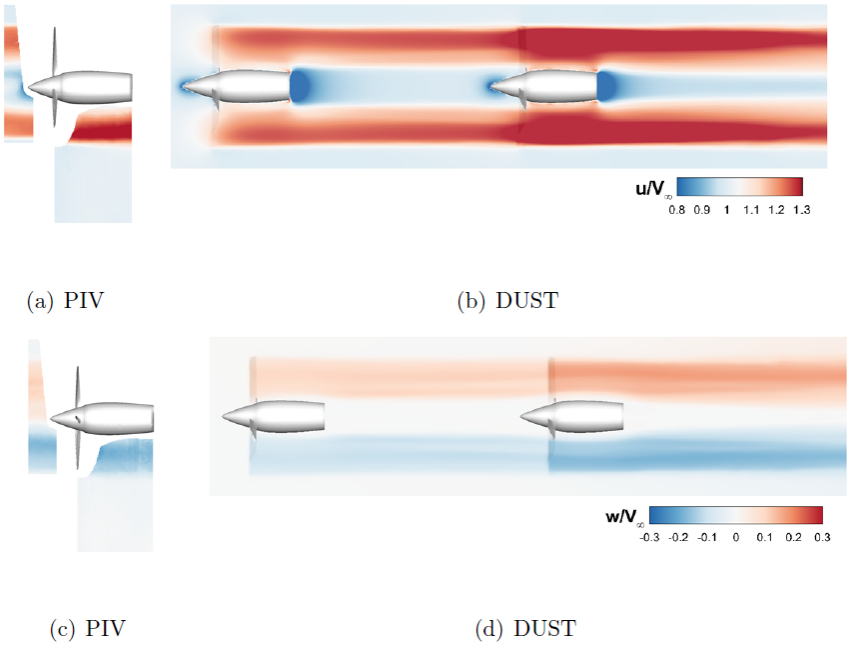

(a) PIV (b) DUST

(c) PIV (d) DUST

Figure 7: Comparison of the averaged freestream and out-of-plane velocity components for the tandem propellers configuration with L_x = 5R and L_y = 0 at J = 0.8, $Re_D = 1.96 \cdot 10^6$, $M_t = 0.325$.

Figure 7 shows the results for the coaxial configuration, i.e. L_y = 0, highlighting the remarkable influence of the front propeller slipstream on the rear propeller disk inflow. A significant acceleration of the rear propeller outer wake region is observed from free-stream velocity component representation. On the other hand, in terms of out-of-plane velocity component, the ingestion of the front propeller slipstream produces a non-negligible magnitude increase of swirl with respect to front propeller flow field. Numerical simulations results show a quite good agreement with experiments, capturing both velocity fields and a symmetric flow pattern. In particular, numerical simulation allows to access a larger field of view with additional insights on the flow field. Indeed, DUST results show a slipstream core contraction of the rear propeller higher with respect to the front one.

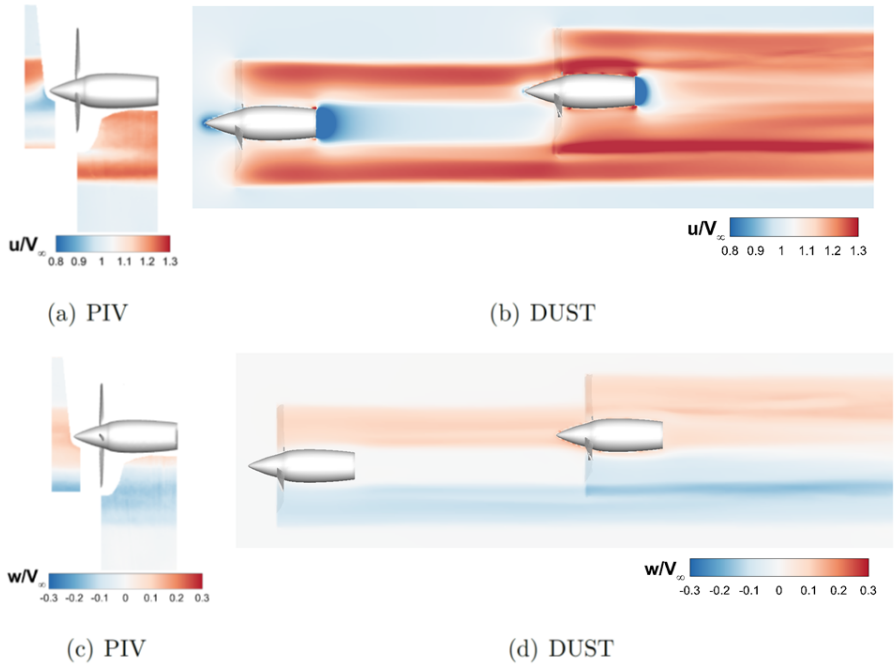

Figure 8: Comparison of the averaged freestream and out-of-plane velocity components for the tandem propellers configuration with L_x = 5R and L_y = 0.5R at J = 0.8, $Re_D = 1.96 \cdot 10^6$, $M_t = 0.325$.

A more evident effect of the aerodynamic interaction between the propellers is visible when increasing the separation distance between them to L_y = 0.5R. In this configuration an asymmetric behaviour of the rear propeller inflow is observed (see Fig. 8), which is consequently reflected in the rear propeller wake. In particular, the upper region of the front propeller slipstream is forced to overcome the rear propeller nacelle with an upward deviation. This produces an accelerated flow region due to the spinner curvature over the rear nacelle. The same region is also characterised by a small positive increase of the out-of-plane velocity component (see Fig. 8c). The observation of PIV measurements highlights also that the lower inner portion of the front propeller wake is interacting with the lower region of the rear propeller wake. The outcome of the interaction is a non-uniform accelerated flow region that is expanding as long as the wake progresses. This feature can be observed in the free-stream velocity component representation, but also the out-of-plane velocity component is characterised by an increased negative value, as particularly evident from the numerical results (see Fig. 8d).

The analysis of the results for the configuration with L_y = 1R clearly shows that the upper portion of the rear propeller disk is not influenced by the front propeller wake. On the other hand, the lower portion of the rear propeller disk, is fully immersed in the front propeller wake, showing major effects with a strongly accelerated flow region in this area (see Fig. 10a). Moreover, in this configuration the lower portion of the rear propeller disk is typically affected by negative swirl velocity, while the interaction with the upper portion of the front propeller slipstream, characterised by positive swirl velocity, modifies significantly the flow field. The outcome is a strong reduction of the out-of-plane velocity component in the wake region past the lower portion of the rear propeller disk compared to other configurations (see Fig. 10c). Numerical simulations allowed to access the global picture of the flow field, showing the front propeller wake which is dragged downward in this configuration and the lower portion of the rear wake that is strongly affected by the acceleration imposed by the front propeller slipstream. Therefore, the rear propeller wake core shows higher level of asymmetry with respect to previous configurations and the lower portion of the rear wake is dragged downward. The complexity of the flow region is testified also by the observation of the out-of-plane velocity field shown in Fig. 10d, which highlights the coexistence of flow regions with opposite sign velocity component.

In order to investigate the vortex-vortex interaction occurring for tandem propellers configuration, the instantaneous flow fields are analysed and compared, considering the phase-locked PIV measurements results and numerical simulations. In particular, Fig. 10 shows the comparison of the out-of-plane component of vorticity evaluated for blade azimuthal angle $\psi = 170°$. The zero blade azimuthal angle is considered in the present work with propeller blade axis aligned vertically. Moreover, in order to obtain a three-dimensional representation of the vortices behaviour, numerical results are presented combining iso-surface of Q-criterion and vorticity contours. In the instantaneous flow field comparison experimental data were obtained by phase-averaging the phase-locked PIV measurements triggered by the azimuthal position of the rear propeller blade, with the front propeller in free-run condition. On the other hand, numerical simulations were performed considering the two tandem propellers with synchronised blade azimuthal phase.

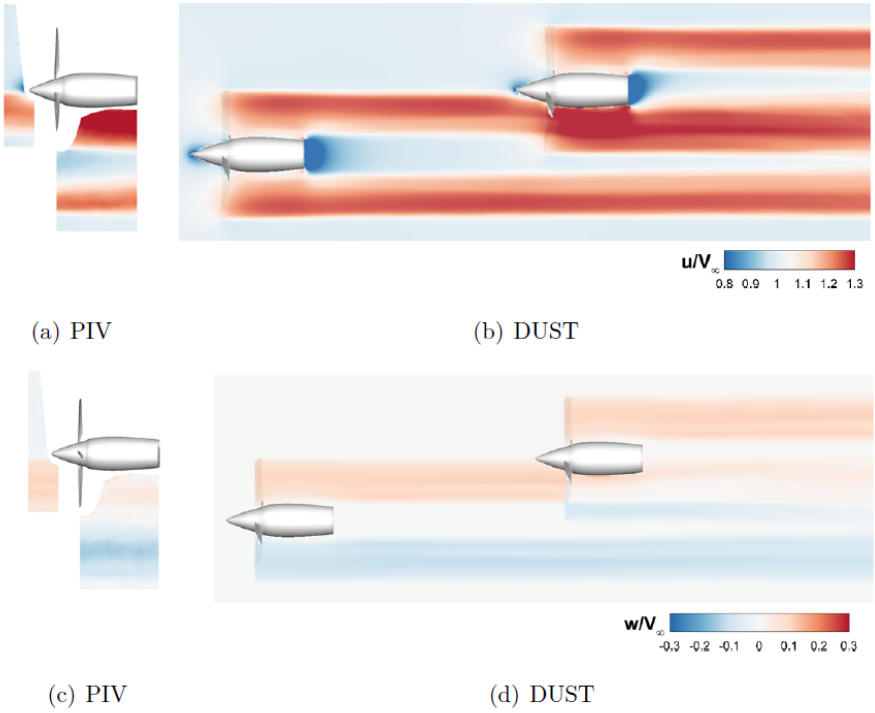

(a) PIV (b) DUST

(c) PIV (d) DUST

Figure 9: Comparison of the averaged freestream and out-of-plane velocity components for the tandem propellers configuration with L_x = 5R and L_y = 1R at J = 0.8, $Re_D = 1.96 \cdot 10^6$, $M_t = 0.325$.

For coaxial propellers configurations, the phase-averaged PIV results show distinctly the pattern of front propeller blade-tip vortices moving towards the rear propeller disk. The interaction with the rear propeller blade-tip vortices results in a reduced vorticity intensity. The observation of numerical results for the same configuration clearly highlights a pattern of vortex couples in the rear propeller wake. The interaction happening at the level of the vortex couple leads to a faster loss of coherence of the vortical structures, as highlighted by Q-criterion iso-surfaces (see Fig. 10b). Blade root vortices are also visible in the instantaneous flow fields representation and similar considerations can be made thanks to the axial-symmetry characterising the coaxial configuration.

The analysis of PIV measurements for the configuration with L_y = 0.5R shows a moderate higher level of dissipation compared to the previous configuration as the rear propeller vortices are immersed in the accelerated flow region related to the influence of the front propeller slipstream. This is evident while observing the lower portion of the rear propeller wake in Fig. 10c, where the blade-tip vortices of the rear propeller interact with front propeller blade root vortices. The effect is confirmed by the analysis of numerical results which also show a loss oh coherence of vortical structures in this region (see Fig. 10d). Moreover, numerical simulations show an upward motion of the front propeller upper blade-tip vortices due to the presence of the rear propeller nacelle. As a result of such motion, the front propeller blade-tip vortices interact with the rear propeller blade root vortices with consequent dissipation and loss of coherence.

Results for tandem propeller configuration with L_y = 1R show a turnaround in term of vorticity dissipation with the vorticity level of blade-tip vortices slightly higher compared to previous tandem configurations (see in particular PIV results in Fig. 10e). This evidence is connected with the relative position of vortex traces in the flow field, with the front propeller blade-tip vortices pattern in the lower portion of the wake that is positioned nearly midway between rear propeller blade-tip and root vortices (see Fig. 10f). In addition, the numerical instantaneous flow field for this configuration highlights an intense dissipation process happening at the level of the rear propeller spinner. The blade-tip vortices associated with the upper portion of the front propeller slipstream impinge on the spinner, dissipate and become almost undetectable downstream the rear propeller. Moreover, a vortex-vortex interaction can be observed while considering the lower portion of the rear propeller wake, in which rear propeller blade-tip vortices interact with front propeller root vortices. Consequently, the numerical flow field shown in Fig. 10f points out the fact the the loss of coherence of helical structures represented by Q-criterion isosurfaces is related only to lower the portion of the rear propeller wake, i.e. the one immersed in the front propeller slipstream.

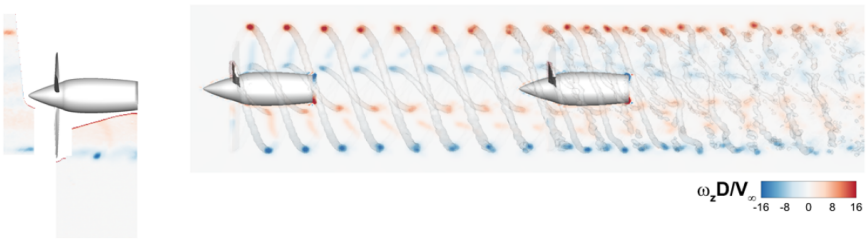

(a) PIV - $L_y = 0$ (b) DUST - $L_y = 0$

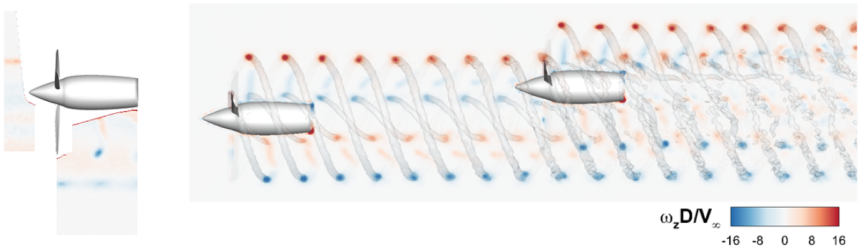

(c) PIV - $L_y = 0.5$R (d) DUST - $L_y = 0.5$R

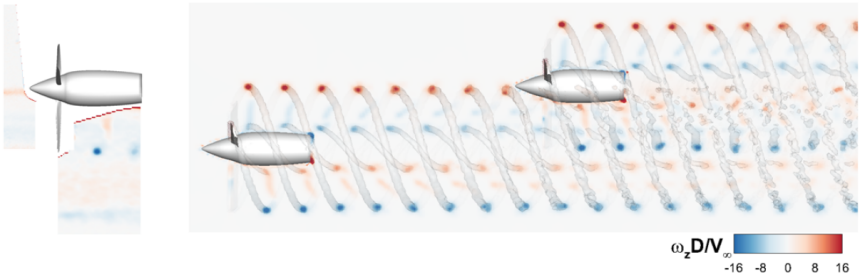

(e) PIV - $L_y = 1$R (f) DUST - $L_y = 1$R

Figure 10: Comparison of the instantaneous out-of-plane vorticity component and iso-surface of Q-criterion, for the single and tandem propellers configurations with L_x = 5R at J = 0.8, $\psi = 170°$, $Re_D = 1.96 \cdot 10^6$, $M_t = 0.325$.

4 CONCLUSIONS

A comprehensive wind tunnel test campaign was performed at Politecnico di Milano to investigate the aerodynamic interaction effects between two tandem propellers with several degree of overlap, reproducing characteristic airplane mode flight conditions for eVTOLs. Loads and flow field measurements were performed to achieve a complete and detailed picture of the phenomena involved in the aerodynamic interaction. Numerical simulations performed the mid-fidelity aerodynamic solver DUST developed at Politecnico di Milano were used to improve the understanding of the flow physics of this complex phenomenon.

Performance measurements highlighted the effects of aerodynamic interaction between the two tandem propellers, with particular focus on the detrimental effects provided on rear propeller performance for different configurations which differed in degree of overlap of the propellers disks. The systematic analysis of the wind tunnel measurements enabled to observe the highest aerodynamic performance losses for the coaxial configuration, which was characterised by a major reduction of the rear propeller thrust in the order of 30% for the current propeller configuration test case. On the other hand, the spectral analysis of the measured thrust signals highlighted that the highest loads fluctuations on rear propeller due to the interaction can be found with a separation distance between the propellers axis equal to one propeller radius. Consequently, the configurations with partial overlap between the propellers disks can produce more severe conditions in terms of acoustic impact.

The stereo PIV surveys performed in wind tunnel enabled to collect details about the flow field characterising the aerodynamic interaction between the tandem propellers. Furthermore, the comparison of the flow fields obtained

through PIV with numerical simulations results enabled to validate the capabilities of the mid-fidelity numerical code used to describe this problem. Consequently, the additional information obtained from simulations allowed to show how the front propeller slipstream modify the rear propeller inflow and wake as a function of the separation distance between the two propellers. In particular, a detailed picture of the complex interaction phenomenon occurring between vortices arrays issued by both blades roots and tips of the tandem propellers was collected and analysed.

Generally speaking, the experimental data base collected through the experimental campaign over a simplified but informative model constitutes a guideline for the design optimisation of eVTOL vehicle configurations and represents a suitable tool for the validation of CFD solvers with different level of fidelity to be used for aerodynamic studies of complete eVTOL aircraft.

Copyright Statement

REFERENCES

[1] Nicholas Polaczyk, Enzo Trombino, Peng Wei, and Mihaela Mitici. A review of current technology and research in urban on-demand air mobility applications. In *Proceedings of the Vertical Flight Society's 6th Annual Electric VTOL Symposium*, Mesa, AZ, USA, 29–31 January 2019.

[2] W. Johnson, C. Silva, and E. Solis. Concept vehicles for vtol air taxi operations. In *Proceedings of the AHS Technical Conference on Aeromechanics Design for Transformative Vertical Flight*, San Francisco, CA, USA, January 16-19 2018. AHS International.

[3] C. Silva, W.R. Johnson, E. Solis, M. D. Patterson, and K. R. Antcliff. Vtol urban air mobility concept vehicles for technology development. In *Proceedings of the AIAA Aviation Technology, Integration, and Operations Conference*, Atlanta, GA, USA, June 25-29 2018. AIAA.

[4] Giovanni Droandi, Monica Syal, and Geoffrey Bower. Tiltwing multi-rotor aerodynamic modeling in hover, transition and cruise flight conditions. In *Proceedings of the 74th Annual Forum*, Phoenix, May 2018. AHS International.

[5] FD Harris. Technical note: Twin rotor hover performance. *Journal of the American Helicopter Society*, 44(1):34–37, 1999.

[6] M Ramasamy. Hover performance measurements toward understanding aerodynamic interference in coaxial, tandem, and tilt rotors. *Journal of the American Helicopter Society*, 60(3):1–17, 2015.

[7] W Zhou, Z Ning, H Li, and H Hu. An experimental investigation on rotor-to-rotor interactions of small uav propellers. In *Proceedings of the 35th AIAA Applied Aerodynamics Conference*, Denver, USA, 5–8 June 2017.

[8] D Shukla and N Komerath. Multirotor drone aerodynamic interaction investigation. *Drones*, 2(4):1–13, 2018.

[9] A Zanotti, R Piccinini, and M Tugnoli. Numerical investigation of the rotor-rotor aerodynamic interaction of evtol configurations by a mid-fidelity approach. In *Proceedings of the 47th European Rotorcraft Forum*, Virtual Event, September 7-9 2021.

[10] Matteo Tugnoli, Davide Montagnani, Monica Syal, Giovanni Droandi, and Alex Zanotti. Mid-fidelity approach to aerodynamic simulations of unconventional vtol aircraft configurations. *Aerospace Science and Technology*, 115:106804, 2021.

[11] Giovanni Droandi, Monica Syal, and Geoffrey Bower. Analysis of the interactional aerodynamics of the vahana evtol using a medium fidelity open source tool. In *Proceedings of the VFS Aeromechanics for Advanced Vertical Flight Technical Meeting*, San Jose, CA, USA, January 21-23 2020. AHS International.

[12] Alex Zanotti and Davide Algarotti. Aerodynamic interaction between tandem overlapping propellers in evtol airplane mode flight condition. *Aerospace Science and Technology*, 124:107518, 2022.

[13] TCA Stokkermans, D Usai, T Sinnige, and Veldhuis LLM. Aerodynamic interaction effects between propellers in typical evtol vehicle configurations. *Journal of Aircraft*, Article in Advance:1–19, 2021.

[14] R. Piccinini. Rotor-rotor aerodynamic interactions for evtol aircraft configurations. Master's thesis, Politecnico di Milano, 2020.

[15] Riccardo Piccinini, Matteo Tugnoli, and Alex Zanotti. Numerical investigation of the rotor-rotoraerodynamic interaction for evtol aircraftconfigurations. *Energies*, 13(22):1–28, 2020.

[16] D. Algarotti. Experimental-numerical investigation of the aerodynamic interaction between tandem propellers in evtol airplane mode. Master's thesis, Politecnico di Milano, 2021.